Journal of Carbon Research

MDPI

Article

Exploring Metal Cluster Interactions with Functionalized Graphene via Molecular Dynamics Simulation

Miriam Roldán-Matilla [1], Arisbel Cerpa-Naranjo [2] and Isabel Lado-Touriño [2,*]

[1] Professional Formation Centre, European University of Madrid, Villaviciosa de Odón, 28670 Madrid, Spain; miriam.roldan@universidadeuropea.es
[2] Department of Engineering, Architecture, Engineering and Design Faculty, European University, Villaviciosa de Odón, 28670 Madrid, Spain; arisbel.cerpa@universidadeuropea.es
* Correspondence: misabel.lado@universidadeuropea.es

Abstract: This study investigates the interaction between copper (Cu) and silver (Ag) clusters and graphene-based materials using molecular dynamics simulations. It focuses on how graphene oxidation and aminated polyethylene glycol (PEG-NH_2) functionalization influence interaction strength and cluster dynamics. The analysis includes pristine graphene (PG), low-oxidized graphene oxide (GOL), and PEGylated graphene oxide (GO-PEG-NH_2). The results reveal that clusters on PG exhibit high mobility, while GO-PEG-NH_2 significantly restricts mobility due to strong interactions, as evidenced by highly negative interaction energies. GO-PEG-NH_2 systems also display pronounced subdiffusive behavior ($\alpha < 1$), indicating strong binding and constrained motion. These findings underscore the critical role of PEG-NH_2 functionalization in controlling cluster diffusion, paving the way for innovative designs in biomedical and catalytic nanocarrier applications.

Keywords: graphene oxide; PEGylation; molecular dynamics; clusters; diffusion; interaction energy; copper; silver; surface functionalization

check for updates

Citation: Roldán-Matilla, M.; Cerpa-Naranjo, A.; Lado-Touriño, I. Exploring Metal Cluster Interactions with Functionalized Graphene via Molecular Dynamics Simulation. *C* **2024**, *10*, 107. https://doi.org/10.3390/c10040107

Academic Editor: Giuseppe Cirillo

Received: 22 November 2024
Revised: 13 December 2024
Accepted: 16 December 2024
Published: 18 December 2024

Copyright: © 2024 by the authors. Licensee MDPI, Basel, Switzerland. This article is an open access article distributed under the terms and conditions of the Creative Commons Attribution (CC BY) license (https://creativecommons.org/licenses/by/4.0/).

1. Introduction

Graphene's exceptional properties have led to a wide range of applications across various fields. In electronics, its outstanding electrical conductivity enables the development of faster and more efficient transistors and sensors [1,2]. In the energy sector, graphene is being explored for use in supercapacitors and batteries, significantly enhancing energy storage capabilities [3]. Its mechanical strength and light weight make it an ideal candidate for creating advanced composite materials in aerospace and automotive industries [4]. Additionally, in biomedicine, graphene biocompatibility and high surface area facilitate drug delivery systems and biosensors, offering promising solutions for targeted therapies and diagnostics [5–8]. Overall, graphene versatility and remarkable characteristics continue to drive innovation and open new avenues in multiple disciplines.

Graphene oxide (GO), a material derived from graphene, stands out as a remarkable material due to its unique functional groups, which significantly enhance its versatility in various applications, improve GO's dispersibility in a range of solvents, and allow for extensive surface modifications [9]. This adaptability makes GO an excellent candidate for integrating with different chemical groups, facilitating innovative solutions in fields such as drug delivery, biosensing, and advanced composites [10–12]. By leveraging these properties, researchers can develop multifunctional materials that can address complex challenges across multiple domains, paving the way for advancements in technology and healthcare. GO serves as an excellent platform for the adsorption of various therapeutic agents due to its high surface area, which allows for a significant loading capacity, enabling GO to effectively encapsulate drugs, nanoparticles, and other therapeutic molecules. The presence of functional groups, such as hydroxyl and carboxyl group, enhances its interaction with these agents, promoting strong adhesion and stability. As a result, GO can be

utilized in drug delivery systems [13], bioimaging and diagnostics [14], or antibacterial applications [15], among others. This makes GO a promising candidate for biomedical applications, although further research is needed to address safety, standardization, and regulatory concerns.

The high specific surface area of graphene enables strong interaction with various types of nanoparticles, improving its ability to interact specifically with biological systems. For instance, Au nanoparticles are commonly used to functionalize graphene-derivatives for biosensing applications [16], where their combined electrical and optical properties improve detection sensitivity for biomolecules. Ag and Cu nanoparticles, known for their antimicrobial properties, are used in combination with graphene derivatives in wound dressings to prevent infections [17–21]. Additionally, magnetic nanoparticles, such as iron oxide, can be anchored onto graphene for targeted drug delivery, where their magnetic properties allow for precise control and positioning within the body [22].

PEGylation, or the attachment of polyethylene glycol (PEG) chains, to graphene derivatives offers several beneficial effects for biomedical applications. This modification enhances the biocompatibility and stability of graphene-based materials, making them more suitable for use within the human body [23]. For example, PEGylated GO has shown reduced toxicity and improved circulation time in the bloodstream, which is essential for applications in drug delivery. By PEGylating graphene, researchers have also increased its dispersibility in aqueous solutions, which is crucial for injectable therapies. Furthermore, PEGylated graphene has been used effectively in photothermal therapy for cancer treatment [24], as the PEG layer helps avoid rapid clearance by the immune system, allowing graphene to accumulate at tumor sites and convert light into heat to target cancer cells. PEGylation of graphene derivatives also can help immobilize therapeutic nanoparticles on its surface, optimizing drug delivery systems by enabling sustained release. This ability to anchor nanoparticles securely on PEGylated graphene surfaces significantly expands its versatility in medical treatments and diagnostics [25–27].

Among various PEG derivatives, PEG-NH_2 (aminated PEG) stands out for its unique properties compared to non-functionalized PEG and other biocompatible polymers. The terminal amino groups of PEG-NH_2 enable covalent bonding with carboxyl groups on GO surfaces via carbodiimide chemistry [28], resulting in enhanced chemical and thermal stability. While non-functionalized PEG can also form covalent bonds with GO through esterification [29], it lacks the versatility and reactivity of terminal amino groups. PEG-NH_2 facilitates robust and site-specific functionalization, offering improved stability and adaptability—key attributes for biomedical applications in complex environments [30,31].

In catalytic applications, PEG-NH_2 provides a significant advantage due to its pH-responsive behavior. At acidic pH, the amino groups are protonated, acquiring a positive charge that strengthens electrostatic interactions with negatively charged nanoparticles or biomolecules, improving retention and stability on functionalized surfaces. Under neutral or basic conditions, the uncharged amino groups promote weaker van der Waals interactions, allowing for fine-tuned catalytic performance. This dynamic adaptability minimizes nanoparticle aggregation and enhances catalytic activity over multiple reaction cycles [32,33]. Functionalized GO with PEG-NH_2 effectively stabilizes metallic nanoparticles by enhancing dispersion, reducing aggregation, and optimizing active site availability, improving overall catalytic system performance [34].

For drug delivery, PEG-NH_2 surpasses other polymers such as chitosan, hyaluronic acid (HA), polyvinylpyrrolidone (PVP), and polyethyleneimine (PEI). Chitosan, while biodegradable and antimicrobial, suffers from poor solubility and limited stability under dynamic conditions. HA, though cell-compatible and ideal for hydrophilic drug loading, lacks chemical stability in harsh environments and offers fewer reactive sites [35,36]. PEI-abundant amino groups allow dense functionalization with GO and strong coordination with metallic nanoparticles, making it highly effective for catalytic applications. However, its cytotoxicity limits its use in biomedical contexts [37,38]. PVP, while biocompatible and capable of stabilizing GO and nanoparticles through non-covalent interactions, lacks reactive groups for stable covalent

bonding, making it suitable only for simpler systems [39,40]. PEG-NH_2 combines the strengths of the previously mentioned polymers, offering biocompatibility, chemical reactivity, and functional versatility. It enhances nanoparticle dispersion, minimizes aggregation, and maximizes catalytic efficiency. In drug delivery, it enables both covalent attachment of activated biomolecules and non-covalent interactions, ensuring precise, controlled functionalization. As a result, PEG-NH_2 is well-suited for advanced therapeutic systems and GO functionalization, outperforming other polymers in complex applications [31–41]. On the other hand, the role of amino groups (-NH_2) in PEG-NH_2 parallels their functionality in metal–organic frameworks (MOFs), where groups like -NH_2, -OH, and -COOH enhance encapsulation through hydrogen bonding, improve stability via covalent conjugation, and regulate drug release by modulating carrier–drug interactions [42].

Molecular simulation methods, both those based on first principles and classical mechanics, possess powerful capabilities for studying atomic-level systems, particularly in understanding the interactions between various nanoparticles and graphene derivatives. First-principles methods, such as density functional theory (DFT), allow for highly accurate predictions of electronic properties and can reveal insights into the bonding characteristics between nanoparticles and graphene [43,44]. These techniques are invaluable for exploring how different nanoparticle types, such as gold or silver, interact with the graphene surface, providing detailed information on adsorption energies and stability [45,46]. On the other hand, classical molecular dynamics (MD) simulations offer a complementary approach by enabling the study of larger systems over extended timescales. This allows researchers to investigate the dynamic behavior of nanoparticle–graphene assemblies, including diffusion, aggregation, and the effects of environmental factors [47,48]. Together, these simulation techniques provide a comprehensive framework for understanding the fundamental interactions at play, guiding the design of advanced nanomaterials for various applications in fields like biomedicine and electronics.

In this study, we performed molecular dynamics (MD) simulations to investigate the interactions between various graphene-based materials and small clusters of Cu and Ag. We examined how the oxidation level of GO and the incorporation of PEG-NH_2 chains, featuring amino groups at both ends, influence the interaction strength with graphene sheets. Our goal is to identify the characteristics of an efficient cluster carrier that can interact strongly with nanoparticles. MD simulations enable us to uncover the underlying mechanisms of these interactions at the molecular level, providing insights into the design of enhanced materials for diverse applications

2. Materials and Methods

2.1. Models

The molecular models used to study interactions between Cu and Ag clusters and pristine graphene (PG), low-oxidized graphene oxide (GOL), and PEGylated graphene oxide (GO-PEG) are shown in Figure 1. Details of these graphene-based models are provided in Table 1. Thirteen atoms arranged in an icosahedral shape were used to represent the Ag and Cu nanoparticles, a model chosen due to the well-established stability of this geometry for Cu and Ag clusters [49,50]. The size and shape of the cluster can significantly influence the numerical values of the results, although the overall interaction trends are expected to remain unaffected. It is well-established that cluster size and shape impact its electronic structure, thereby affecting its interaction and reactivity with the surface. Accurate determination of these effects would require quantum mechanical calculations using minimally simplified models that still capture the system complexity. However, such calculations are impractical for the large-scale models considered in this study. The graphene sheet dimensions were 36×36 Å^2 for PG and all other graphene-derived materials. To create the GO model, the PG surface and edges were randomly decorated with hydroxyl, epoxide, and carboxyl groups, resulting in a final oxygen content of 17.57% by weight. The PEGylated graphene oxide (GO-PEG) model was created by adding four PEG chains to the surface of the GO model. Each PEG chain had a degree of

polymerization of 10 and featured terminal amino groups, resulting in PEG-NH_2. The PEG chains were attached at carefully selected sites to ensure uniform surface coverage.

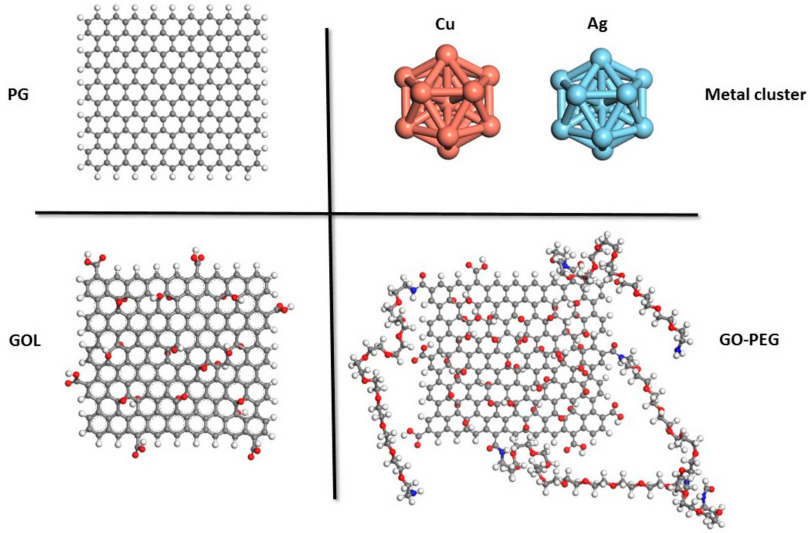

Figure 1. Molecular models used to study interactions between Cu and Ag clusters and graphene-based materials. Atom colors: carbon (C) in gray, hydrogen (H) in white, copper (Cu) in brown, silver (Ag) in light blue, oxygen (O) in red, and nitrogen (N) in blue. Graphene sheet dimensions: 36 × 36 $Å^2$; Cu cluster diameter: 4.18 Å; Ag cluster diameter: 4.94 Å (maximum vertex-to-vertex distance).

Table 1. Detailed information on the molecular models used.

System	Chemical Formula	Additional Data
PG	$C_{190}H_{38}$	
GOL	$C_{196}H_{47}O_{32}$	17.57 (percentage by weight of O)
GO-PEG	$C_{289}H_{245}N_8O_{100}$	4 PEG chains, degree of polymerization n = 10

The initial structures for this study were built by positioning a cluster 12 Å above the geometric center of each carbon-based surface. The clusters were then placed within a three-dimensional periodic simulation cell with dimensions of 40 × 40 × 40 $Å^3$. Next, 2375 water molecules were added around the clusters and graphene-derived materials to fully hydrate the structures. Figure 2 shows the initial configurations of several systems simulated in this study.

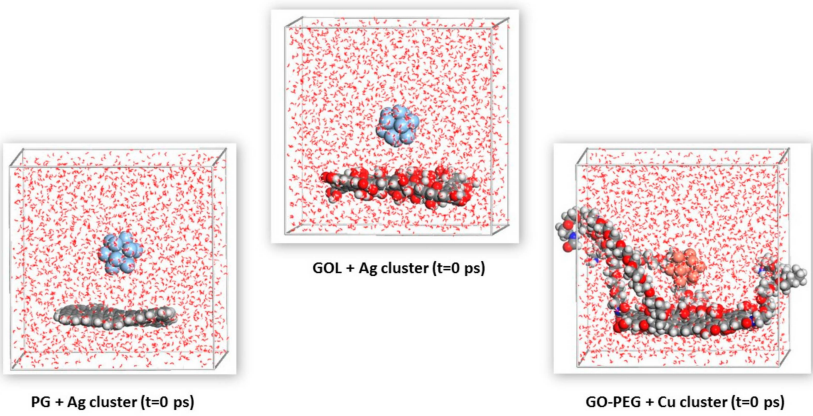

Figure 2. Models used to investigate interactions between metallic clusters and graphene-based materials. Atom color scheme: carbon (C) in gray, hydrogen (H) in white, copper (Cu) in brown, silver (Ag) in light blue, oxygen (O) in red, and nitrogen (N) in blue. The water molecules are represented as red lines.

2.2. Calculation Method

Molecular dynamics (MD) simulations were conducted using the Forcite module in Materials Studio 9 software [51] within the NVT ensemble, maintaining a constant number of particles (N), volume (V), and temperature (T) over a simulation period of 1000 ps. Temperature was kept constant at 298 K using a Nosé–Hoover thermostat [52,53]. Electrostatic and van der Waals interactions were calculated using an atom-based summation method with a cut-off distance of 12.5 Å. Atomic interactions were modeled using the COMPASSII force field, which is parameterized based on experimental and ab initio data. This allows for the precise prediction of various gas-phase and condensed-phase properties for a wide range of organic and inorganic materials [54], including graphene and graphene-based systems [55,56].

2.2.1. Interaction Energies

The interaction energies (ΔE) between clusters and the graphene-based surface were calculated using the following Equation:

$$\Delta E = E_{GBM-cluster} - (E_{GBM} + E_{cluster}) \tag{1}$$

where $E_{GBM-cluster}$ represents the average equilibrium potential energy of the graphene-based material interacting with the cluster, while E_{GBM} and $E_{cluster}$ are the average equilibrium potential energies of the isolated graphene-based materials and cluster, respectively. These energies were determined by averaging values over the final 300 ps of each simulation. A more negative energy interaction indicates a stronger interaction between the cluster and the graphene-based surface.

2.2.2. Mean-Squared Displacement (MSD)

The mean-squared displacement (MSD) of the clusters, which quantifies the spatial extent of their random motion, was calculated based on their positions throughout the simulation duration as follows:

$$MSD(t) = \frac{\sum_{i=1}^{N} \langle |\vec{r}_i(0) - \vec{r}_i(t)|^2 \rangle}{N} \tag{2}$$

where $\vec{r}_i(0)$ denotes the initial reference position of the cluster, $\vec{r}_i(t)$ is its position at time t, and N is the total number of atoms in the cluster. The MSD was calculated based on the particle positions along their trajectory using a time step of 5 ps, providing insights into the effective displacement speed of nanoparticles over the timescale considered, which is inversely related to the strength of their interaction with the surface. A lower MSD indicates stronger interaction and therefore restricted mobility, whereas a higher MSD suggests weaker interaction and increased translational mobility. Furthermore, the relationship between MSD and time (t) can be expressed as follows:

$$MSD = K_\alpha t^\alpha \tag{3}$$

where K_α represents the generalized diffusion coefficient, and α denotes the diffusion exponent, both of which are key parameters for understanding fundamental diffusion processes [57,58]. The generalized diffusion coefficient K_α quantifies the overall rate of particle displacement and reflects the influence of the surrounding environment, including surface interactions and the presence of structural barriers. A higher K_α value indicates increased translational mobility of nanoparticles, whereas a lower value suggests restricted movement, often due to strong interactions or environmental constraints. The diffusion exponent α characterizes the type of diffusion and plays a crucial role in elucidating the influence of surface properties on nanoparticle dynamics. Specifically, this relationship aligns with the anomalous diffusion model, where the value of α determines the nature of the diffusion process: for normal diffusion, $\alpha = 1$, indicating random, unrestricted movement, and suggesting that the nanoparticles experience negligible interactions with the surface. In contrast, for subdiffusive

behavior, $0 < \alpha < 1$, the movement of the nanoparticles is hindered due to strong interactions or structural barriers within the surface. For superdiffusive behavior, $\alpha > 1$, the nanoparticles exhibit enhanced movement, driven by weak surface interactions or favorable conditions that promote directed or accelerated motion.

Using the anomalous diffusion model enables a comprehensive understanding of how surface functionalization affects nanoparticle mobility. By examining the relationship between the generalized diffusion coefficient K_α, the diffusion exponent α, and the interaction energies, this approach offers valuable insights into the system dynamics and the nature of interactions between nanoparticles and graphene-based surfaces.

2.2.3. Diffusion Data Analysis

To analyze the mobility of the metal clusters on the graphene-based surfaces, the MSD of the clusters center of mass over the simulation time was computed. Subsequently, the MSD data as a function of time were fitted to an anomalous diffusion model, allowing for the extraction of the generalized diffusion coefficient K_α and the diffusion exponent α.

The fitting model used corresponds to the general Equation (3). To determine the parameters K_α and α, the MSD data as a function of time were fitted using nonlinear regression [59]. The "*curve_fit*" function from the *SciPy* library in Python 3.13 was employed, enabling nonlinear fitting by minimizing the mean-squared error between the calculated data and the theoretical model. The fitting process was carried out under constraints to ensure the validity of the parameters: K_α was restricted to positive values, and α was limited to the range [0, 2] [57]

The fitting was performed for each combination of carbon-based material and cluster (PG + Cu, PG + Ag, GOL + Cu, GOL + Ag, GO-PEG + Cu, and GO-PEG + Ag). The values of the parameters (K_α and α), along with their associated uncertainties, were obtained from the covariance matrix provided by "*curve_fit*". The uncertainties were calculated as the square root of the diagonal elements of the covariance matrix, representing the precision of the fitting for each parameter.

To validate the fit and analyze the data, scatter plots of the MSD values obtained from the simulation versus time were generated, along with the fitted curves for each system. Python software, along with the NumPy, SciPy, and Matplotlib libraries, was employed for data processing, nonlinear fitting, and graphical visualization of the results. These analyses provided insights into how the interaction between the clusters and the surface influences the mobility of the clusters, and how the functionalization of graphene significantly affects diffusion. These findings were then correlated with the interaction energy values.

3. Results

3.1. Interaction Energies

The interaction energy values (ΔE) obtained from Equation (1) are shown in Figure 3, and the variation in interaction energy with functionalization is summarized in Table 2.

Table 2. Analysis of the variation in ΔE with functionalization.

Functionalization	Cu	Ag	
	Variation in ΔE (kcal/mol)	Variation in ΔE (kcal/mol)	
Oxidation (PG → GOL)	−120.36	−138.77	Ag shows a greater reduction in interaction energy compared to Cu, indicating a higher affinity of Ag towards GOL.
PEGylation (GOL → GO-PEG)	−139.62	−100.70	Cu shows a greater decrease in energy with PEGylation, suggesting that PEGylation has a greater effect on the interaction of Cu.

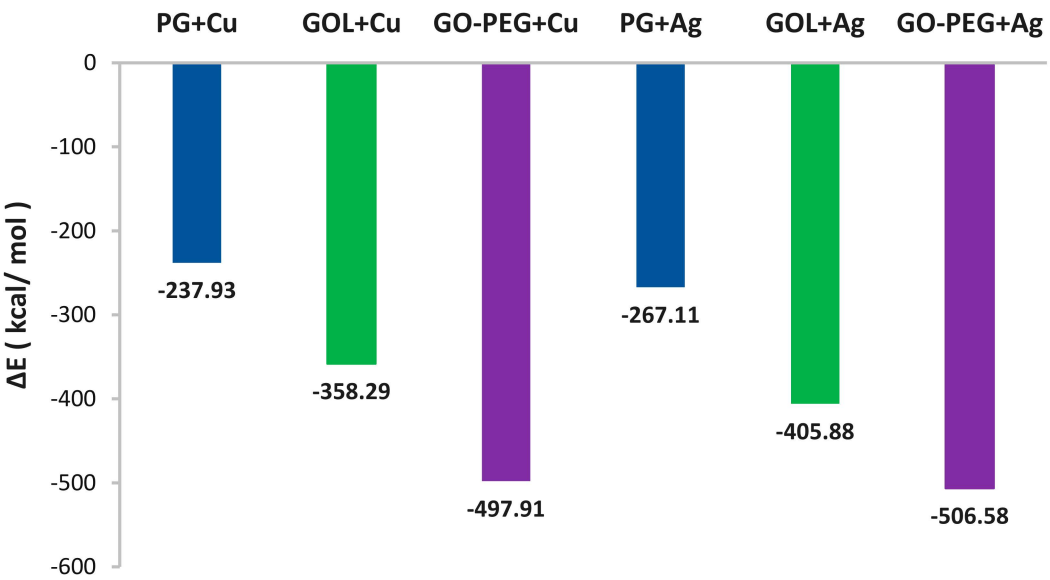

Figure 3. Interaction energies for the adsorption of Cu and Ag clusters on PG and functionalized graphene-based materials.

The data in Figure 3 indicate that the interaction strength depends on both the chemical nature of the cluster and the functionalization of the graphene-based material. In all cases, Ag shows a stronger interaction with the graphene surface than Cu. Surface functionalization enhances these interactions, with PEGylation contributing to a slightly stronger effect. The addition of functional groups to the graphene surface increases adsorption capacity due to improved compatibility by providing more binding sites. PEG chains further contribute by immobilizing the metallic nanoparticles and restricting their movement across the surface, as noted in similar studies by Madhavi et al. [60].

The oxidation level of GO is also a key factor in determining interaction strength. A previous unpublished study combining experimental results and simulations [34] observed interaction energy values of −462.05 kcal/mol for Cu and −485.29 kcal/mol for Ag on a GO surface with 30% oxidation. This suggests that higher oxidation increases the density of functional groups, resulting in more binding sites and leading to stronger interactions.

Both oxidation and PEGylation enhance the affinity of metallic clusters for the graphene surface, though the relative impact varies depending on the metal type, as shown in Table 2. Ag is more sensitive to oxidation, while Cu is more influenced by PEGylation. In PEGylated systems, the interaction energy is more negative for Ag (−506.58 kcal/mol) than for Cu (−497.91 kcal/mol), indicating a stronger affinity of Ag for the PEGylated surface. However, Cu exhibits a greater overall reduction in interaction energy with functionalization (−260.98 kcal/mol for Cu vs. −239.47 kcal/mol for Ag), suggesting that PEGylation has a more pronounced effect on Cu interaction with the surface. However, these results should be interpreted with caution. Additional computational studies with varied configurations are needed to confirm these trends and further assess Cu potential for establishing additional interactions.

3.2. Final Configurations of the Metallic Clusters

The final configurations of all the systems studied are shown in Figure 4. It is evident that the clusters remained close to the surface at the end of the simulation.

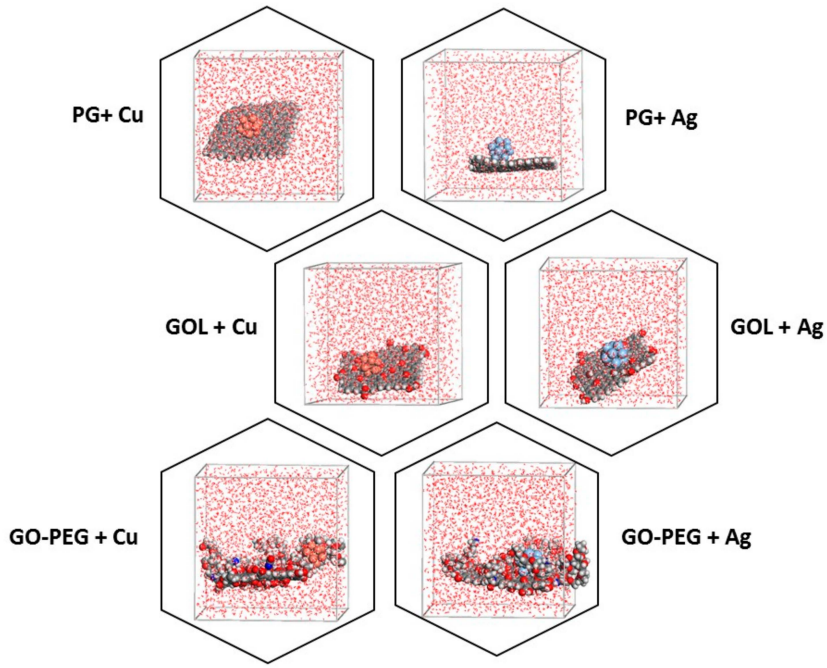

Figure 4. Final positions of Cu and Ag clusters on pristine and functionalized graphene surfaces after 1000 ps of simulation time. Color codes: C—gray, H—white, Cu—brown, Ag—light blue, O—red, N—blue.

3.3. Radial Distribution Functions

To study the position of the cluster relative to the surface, the radial distribution function (RDF) of these structures was calculated for all configurations over the last 300 ps of the simulation. The results obtained are shown in Figure 5.

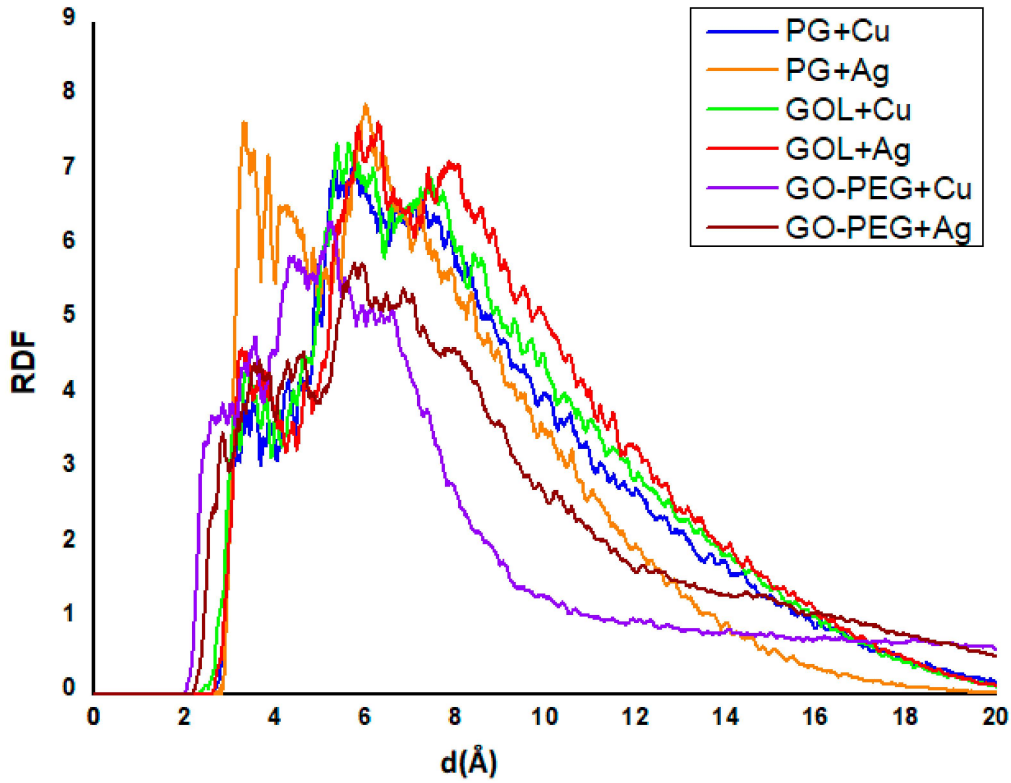

Figure 5. RDF between the center of mass of the cluster and the surface of graphene-derived materials.

For small distances (up to approximately 6 Å), the RDF of all systems displays two peaks with varying intensities. The first peak represents the shortest observed distance, indicating the closest approach between the clusters and the surface, with peak locations varying among systems based on interaction strength. The second peak corresponds to a slightly larger coordination distance, reflecting additional structural arrangements influenced by cluster type and surface functionalization. These peak positions, detailed in Figure 6, illustrate the distance variations that reflect differences in cluster–material affinities across the systems. Notably, the position of the first peak—indicating the minimum distance between the cluster and the graphene-based material—correlates well with the interaction energies presented in Figure 3. Accordingly, the PEGylated systems exhibit the shortest distances for both Ag and Cu clusters (2.83 Å), while PG systems show larger separation distances (3.57 Å).

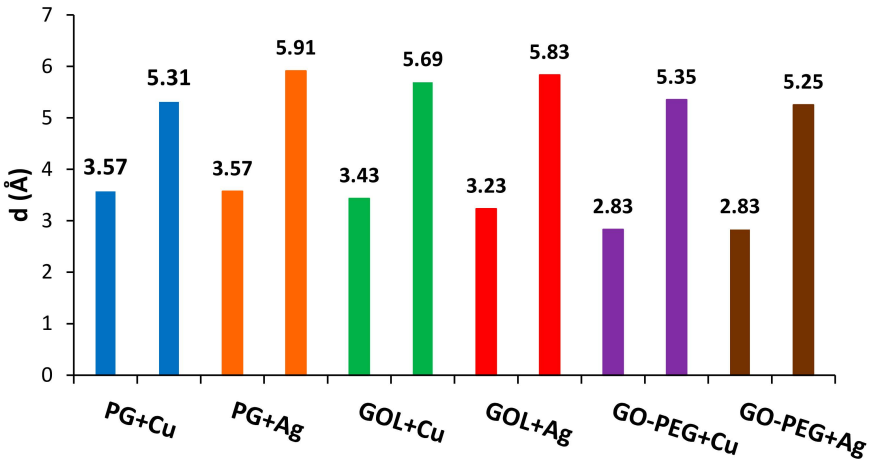

Figure 6. Positions of the first two peaks of the RDF between the clusters and graphene-derived material.

3.4. Dynamics

Figure 7 presents the adsorption time plots for all systems. In each case, the clusters diffuse toward the graphene material and ultimately adsorb onto its surface. The final distance between the cluster center of mass and the basal plane of the surface—measured using only the surface C atoms for consistent comparison across systems—stabilized around 400 ps from the start of the simulation for all systems

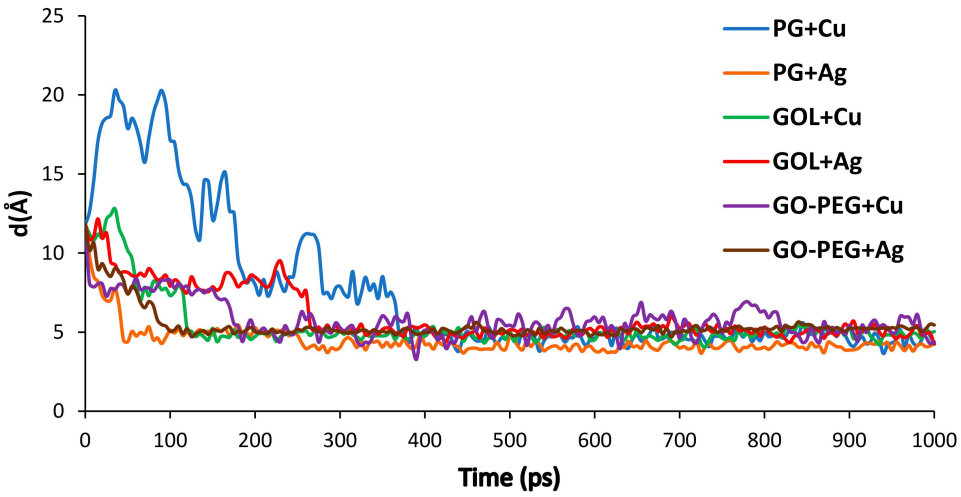

Figure 7. The time-dependent variation in the distance between the cluster center of mass and the surface of the graphene-derived material.

Figure 8 presents the MSD of the cluster center of mass over the simulation duration. Clusters interacting with PG showed the highest MSD values, reflecting the weak attraction from PG, which allowed for continuous movement across the surface. In contrast, functionalization of the graphene sheet led to a significant reduction in MSD values, with the effect most pronounced in PEGylated GO systems. These lower MSD values suggest that clusters near the functionalized surface were less mobile, likely due to stronger interactions. The PEG chains appeared to trap the clusters, restricting their movement across the surface.

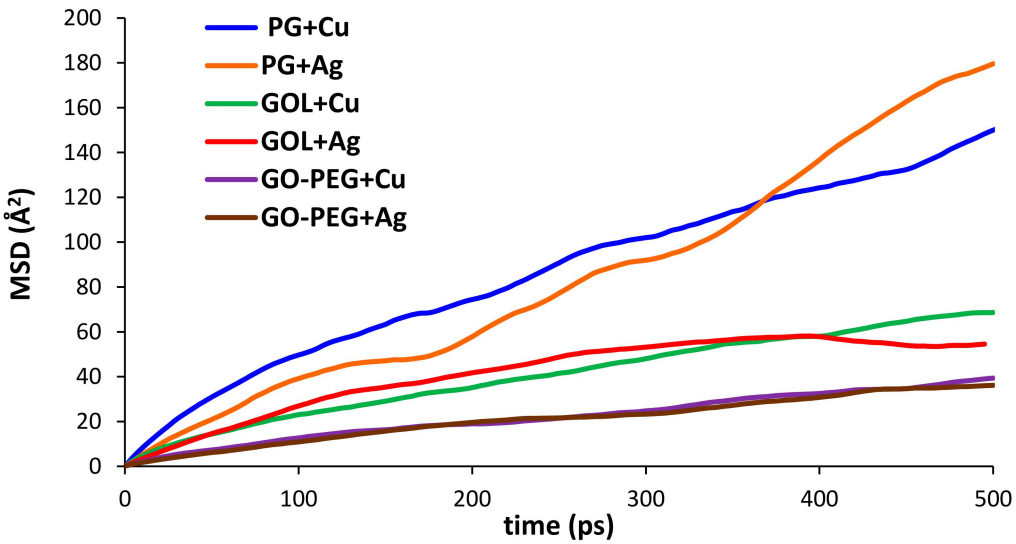

Figure 8. MSD of the cluster center of mass versus the simulation length.

The MSD values align closely with the interaction energies: clusters exhibiting greater mobility correspond to lower interaction energies. This finding is consistent with previous studies. Gervilla et al. [61,62] investigated the diffusion of Cu and Ag clusters on PG using both ab initio and molecular dynamics simulations, observing that clusters moved freely across the graphene surface without becoming trapped at adsorption sites. They attributed this behavior to the flat potential energy landscape on the surface, which facilitates cluster diffusion. Manade et al. [63] reached similar conclusions.

The functionalization of graphene-based surfaces significantly impacts the diffusion behavior of Cu and Ag clusters, as evidenced by the diffusion parameters derived from non-linear fitting (Table 3). The analysis reveals that both PEGylation and oxidation effectively restrict cluster movement, indicating strong interactions that limit mobility.

Table 3. Diffusion parameters for metal clusters on graphene-based surfaces.

System	$K_\alpha (\frac{Å^2}{ps})$	Uncertainty in K_α $(\frac{Å^2}{ps})$	α	Uncertainty in α
PG + Cu	2.0416	±0.0487	0.6859	±0.0041
GOL + Cu	0.8570	±0.0181	0.7067	±0.0036
GO-PEG + Cu	0.4019	±0.0204	0.7316	±0.0087
PG + Ag	0.1466	±0.0191	1.1409	±0.0220
GOL + Ag	2.7306	±0.2942	0.5057	±0.0188
GO-PEG + Ag	0.3575	±0.0189	0.7441	±0.0091

For the PG + Cu system, the diffusion parameters are $K_\alpha = (2.0416 \pm 0.0487)\frac{Å^2}{ps}$ and $\alpha = 0.6859 \pm 0.0041$. The clusters on PG show high mobility with a moderately subdiffusive behavior. However, the limited simulation time (1000 ps) may underestimate mobility, as the clusters may not have fully explored the surface.

For the PG + Ag system, the diffusion parameters are $K_\alpha = (0.1466 \pm 0.0191)\frac{\text{Å}^2}{\text{ps}}$ and $\alpha = 1.1409 \pm 0.0220$. The Ag cluster displays low mobility despite a superdiffusive α value, which seems contradictory. This inconsistency can be attributed to the non-uniform distribution of functional groups on the functionalized surfaces, which creates varying levels of affinity. These variations lead to an uneven distribution of movement, making it difficult to characterize the system's behavior with a single interaction energy value. In systems where ergodicity breakdown occurs, the observed K_α and α values depend heavily on the simulation time and may not fully represent the average behavior. Ag clusters may become trapped in local high-affinity regions, preventing them from thoroughly exploring the surface, thereby contributing to the breakdown of ergodicity. Structural heterogeneity and limited global exploration exacerbate this phenomenon. Moreover, the simulation time might have been insufficient for Ag clusters to escape local traps and explore the surface uniformly, potentially leading to an underestimation of the K_α value. The uncertainty in the fit ($\pm 0.0191\frac{\text{Å}^2}{\text{ps}}$) also suggests stochastic fluctuations, which may impact the precision of the results [57].

For the GOL + Cu system, the diffusion parameters are $K_\alpha = (0.8570 \pm 0.0181)\frac{\text{Å}^2}{\text{ps}}$ and $\alpha = 0.7067 \pm 0.0036$. The presence of oxygenated functional groups on the GO surface introduces barriers that restrict the mobility of Cu clusters. This results in subdiffusive behavior, highlighting the significant influence of these structural barriers on cluster movement.

In the GOL + Ag system, the diffusion parameters are $K_\alpha = (2.7306 \pm 0.2942)\frac{\text{Å}^2}{\text{ps}}$ and $\alpha = 0.5057 \pm 0.0188$. While the high value of K_α for Ag suggests substantial mobility, the subdiffusive α value indicates notable movement restrictions. This apparent contradiction can be attributed to surface heterogeneities on the functionalized GO, which create regions with varying affinities. These variations result in mobility differences that are not fully captured by the average interaction energy values. Additionally, the limited simulation time likely hinders the clusters ability to explore all regions of the surface, thereby influencing the observed K_α value. The high uncertainty in K_α ($0.2942\frac{\text{Å}^2}{\text{ps}}$) further suggests substantial fluctuations in the data, indicating significant dispersion. This variability affects the precision of the diffusion parameter estimates and underscores the complexity of capturing the dynamic behavior in these systems.

For the GO-PEG + Cu and GO-PEG + Ag systems, the diffusion parameters are $K_\alpha = (0.4019 \pm 0.0204)\frac{\text{Å}^2}{\text{ps}}$ for Cu and $K_\alpha = (0.3575 \pm 0.0189)\frac{\text{Å}^2}{\text{ps}}$ for Ag. PEGylation significantly restricts the mobility of both metals, creating a highly restrictive and indicating limited diffusion due to the strong interactions imposed by the PEGylated surface. The α values, $\alpha = 0.7316 \pm 0.0087$ for Cu and $\alpha = 0.7441 \pm 0.0091$ for Ag, indicate subdiffusive behavior, though they are closer to normal diffusion compared to GOL. This suggests that PEGylation creates a uniform environment, consistently limiting mobility across the surface. However, the breakdown of ergodicity may occur due to the structural characteristics of GO-PEG, where PEG chains could form localized regions with varying affinities. This heterogeneity causes the observed K_α and α values to depend on the observation time, as clusters may not uniformly explore the surface and instead become trapped in specific high-affinity regions. Additionally, the simulation time might be insufficient for the clusters to escape these local traps created by PEG groups, further complicating the interpretation of mobility dynamics [58].

To achieve a more comprehensive understanding of the diffusion process, longer simulation times and a wider range of surface models with diverse characteristics would be necessary. Furthermore, advanced techniques, such as the calculation of electrostatic potentials or Fukui indices, could be utilized to investigate the underlying diffusion mechanisms. Electrostatic potential maps, for instance, can identify regions of electron density and deficiency, while Fukui indices quantitatively assess a molecule propensity for nucleophilic or electrophilic attacks at specific atoms or regions. These properties are essential for analyzing the reactivity, interactions, and electronic behavior of molecular systems. However,

such calculations would require quantum mechanical methods and a reformulation of the models employed in this study.

4. Discussion

It is important to highlight that the calculated interaction energies consider only non-bonding interactions between the clusters and the graphene surface. A more comprehensive understanding of these interactions would require quantum mechanical calculations [50]. The participation of metal d-orbitals in charge transfer processes between the clusters and the surface is possible; however, in many cases, this transfer is weak, with bonding primarily dominated by van der Waals forces. This phenomenon has been confirmed in several studies involving Cu and Ag [64,65].

While MD simulations do not rigorously account for the quantum mechanical nature of interactions between clusters and graphene-derived material surfaces, they provide valuable insights into the dynamic behavior of these systems. Such analyses would be unfeasible with ab initio methods due to the high atomic complexity of these models. The tendency of the clusters to remain close to the surface throughout the simulations suggests strong interactions, consistent with the calculated non-bonding interaction energies. This behavior is in line with previous studies [64,65], which have similarly observed that Cu and Ag clusters on graphene surfaces exhibit interactions primarily governed by van der Waals forces. The results reveal a direct correlation between the interaction energy, MSD, and the diffusion parameters obtained through fitting to the anomalous diffusion model, which includes the generalized diffusion coefficient K_α and the diffusion exponent α.

The interaction energy values (ΔE) reflect the strength of attraction between the clusters and the functionalized surfaces. More negative energy values indicate stronger interactions and, consequently, a higher affinity of the cluster for the surface. This increased attraction restricts the mobility of the clusters, as evidenced by the low values of the diffusion coefficient K_α and subdiffusive behavior ($\alpha < 1$).

For the GO-PEG + Ag system, a highly negative interaction energy ($\Delta E = -506.58$ kcal/mol) was observed, which corresponds to a low value of $\alpha = 0.74$, indicating subdiffusive behavior that reflects strong adsorption of the clusters onto the functionalized surface, along with a lower $K_\alpha = 0.3575 \frac{\text{Å}^2}{\text{ps}}$. In contrast, in systems with weaker interactions, such as PG + Cu ($\Delta E = -237.93$ kcal/mol), the K_α values are higher ($K_\alpha = 2.0416 \frac{\text{Å}^2}{\text{ps}}$), suggesting greater mobility of the clusters and less restricted diffusion behavior.

The non-functionalized systems (PG) exhibited fewer restrictions on the mobility of the metallic clusters compared to the functionalized systems. Oxidation of the surface introduces oxygen functional groups, increasing the interaction energy and, consequently, the affinity of the clusters for the surface. This is reflected in lower K_α values and subdiffusive behavior ($\alpha < 1$). For instance, the GOL + Cu system shows an interaction energy of $\Delta E = -358.29$ kcal/mol, with $\alpha = 0.7067$ and $K_\alpha = 0.8570 \frac{\text{Å}^2}{\text{ps}}$, indicating a significant restriction in mobility.

PEGylation (GO-PEG) results in the most negative interaction energies, reflecting the highest affinity of the clusters for the PEGylated surface. This leads to very restricted mobility, with low K_α values and subdiffusive behavior for both metals. For example, in GO-PEG + Cu, the interaction energy of $\Delta E = -497.91$ kcal/mol and $\alpha = 0.73$ indicates reduced mobility due to the strong interaction of the cluster with the surface.

Despite these correlations, some discrepancies should be considered. Functionalized surfaces, particularly GOL and GO-PEG, exhibit structural heterogeneity due to the uneven distribution of functional groups. This heterogeneity can cause clusters to experience varying levels of affinity depending on the region of the surface they encounter, resulting in variations in mobility that are not captured by an average interaction energy value

The simulations were conducted for a limited time of 1000 ps, which may be insufficient for the clusters to fully explore the surface and escape local traps. This could lead to an underestimation of mobility, particularly in the functionalized systems.

In functionalized systems like GO-PEG, the breakdown of ergodicity could also affect the results. The temporal average of the MSD may not represent the ensemble average behavior, as the cluster may become trapped in specific regions without exploring the entire surface [57]

The uncertainties associated with the values of K_α and α are also significant in some systems. For example, in GOL + Ag, the uncertainty in K_α ($\pm 0.2942 \frac{2}{\text{ps}}$) suggests that the nonlinear fit may not be completely precise due to stochastic fluctuations in the MSD data.

The observed discrepancies highlight the complexity of these systems, which require further analysis, such as longer simulation times or an ergodic analysis, to clarify the inconsistencies and provide a more accurate interpretation of the results. Extending the simulation time would not only provide a more comprehensive analysis by generating additional data but also help reduce errors associated with the statistical calculation of MSD, such as numerical inaccuracies and correlation effects. A longer simulation time would allow for a more detailed examination of the diffusion process, improving the statistical reliability of MSD calculations and minimizing the impact of these errors, ultimately yielding more robust results.

Experimental data from our research validate the simulation results, as detailed in a previously unpublished study that integrates experimental findings and simulations [34]. This study employed a variety of analytical techniques, including scanning electron microscopy (SEM), transmission electron microscopy (TEM), UV–Vis spectroscopy, Fourier-transform infrared spectroscopy (FTIR), thermogravimetric analysis (TGA), and Raman spectroscopy, to confirm the interactions between metallic clusters and functionalized graphene surfaces.

SEM and TEM analyses revealed significant improvements in cluster dispersion and uniformity after PEGylation. UV–Vis spectroscopy demonstrated enhanced optical stability and plasmonic response, while TGA confirmed improved thermal stability resulting from PEG functionalization.

These findings highlight the potential of PEGylated systems for applications requiring precise cluster stability and control, such as drug delivery and antimicrobial technologies.

Further exploration of the physical significance and practical applications of these findings is essential to fully understand their impact in fields like catalysis and drug delivery. The observed reduction in cluster mobility and increased interaction energies due to PEGylation suggest clear advantages for catalytic processes, where immobilized active sites can boost reaction efficiency and selectivity. Similarly, in drug delivery applications, the stability conferred by PEG chains could enhance the controlled release of therapeutic agents by preventing cluster aggregation and ensuring uniform dispersion in biological environments. These effects may also reduce toxicity by minimizing unintended interactions with biological components. Nonetheless, additional experimental validation and application-specific testing are necessary to confirm these advantages and to optimize the design of functionalized graphene systems for targeted uses.

5. Conclusions

MD simulations revealed that the chemical nature of the clusters (Cu, Ag) and modifications to graphene-derived materials significantly influence adsorption and surface mobility. Surface functionalization and increased oxidation levels enhanced the interaction between the clusters and the carbon-based material, while the incorporation of PEG chains further stabilized adsorption, increasing interaction energies and reducing cluster mobility on the surface.

The diffusion analyses of Cu and Ag clusters on PG, GOL, and GO-PEG surfaces shows evidence of anomalous diffusion, with clearly subdiffusive behavior observed on the functionalized surfaces (GOL and GO-PEG). This behavior aligns with the theory of anomalous diffusion described in other studies, where the presence of local traps and energy barriers hinders particle movement. The reduction in α values for GO-PEG compared to

GOL and PG suggests that PEGylation increases the density of functional groups on the surface, enhancing cluster affinity and further restricting their mobility.

Moreover, these results indicate a possible breakdown of ergodicity in the functionalized systems, where the temporal average of MSD may differ significantly from the ensemble average. This suggests that individual cluster trajectories may not fully represent the system's average behavior. Non-ergodic behavior is particularly relevant on surfaces like GO-PEG, where PEG groups enhance cluster retention.

The interaction energy and MSD analysis provide complementary insights into adsorption and diffusion dynamics. The more negative-interaction energy values observed on GO-PEG are directly linked to a significant reduction in α values, confirming that strong interactions limit mobility and promote restricted diffusion. These findings have important implications for applications requiring high affinity and restricted movement of clusters on functionalized surfaces, highlighting the role of surface modifications in designing graphene-based materials for nanomaterials and catalysis.

Future work will focus on exploring the systems while accounting for changes in the electronic states of the species after interaction, which are expected to influence adsorption energies. These changes could arise from factors such as the oxidation of metallic atoms by water or their interactions with surface atoms of the graphene-derived materials. Additionally, longer simulation times will be required to enable a more detailed analysis of diffusive behavior, providing a deeper understanding of the system dynamics. Future studies will also incorporate models that vary the cluster size, position, and initial orientation relative to the surface, allowing for a more comprehensive investigation of their effects on interaction and diffusion properties.

Author Contributions: Methodology, M.R.-M. and I.L.-T.; software, I.L.-T.; validation, M.R.-M., I.L.-T. and A.C.-N.; formal analysis, M.R.-M. and I.L.-T.; investigation, M.R.-M., I.L.-T. and A.C.-N.; resources, A.C.-N.; data curation, M.R.-M. and I.L.-T.; writing—review and editing, M.R.-M. and A.C.-N.; supervision, I.L.-T. and A.C.-N.; project administration, A.C.-N.; funding acquisition, A.C.-N. All authors have read and agreed to the published version of the manuscript.

Funding: This research was funded by Universidad Europea de Madrid, grant number 2024/UEM01.

Data Availability Statement: Data available on request.

Conflicts of Interest: The authors declare no financial/commercial conflicts of interest.

References

1. Xue, M.; Mackin, C.; Weng, W.-H.; Zhu, J.; Luo, Y.; Luo, S.-X.L.; Lu, A.-Y.; Hempel, M.; McVay, E.; Kong, J. Integrated biosensor platform based on graphene transistor arrays for real-time high-accuracy ion sensing. *Nat. Commun.* **2022**, *13*, 5064. [CrossRef] [PubMed]
2. Ono, T.; Okuda, S.; Ushiba, S.; Kanai, Y.; Matsumoto, K. Challenges for Field-Effect-Transistor-Based Graphene Biosensors. *Materials* **2024**, *17*, 333. [CrossRef]
3. Olabi, A.G.; Abdelkareem, M.A.; Wilberforce, T.; Sayed, E.T. Application of graphene in energy storage device—A review. *Renew. Sustain. Energy Rev.* **2021**, *135*, 110026. [CrossRef]
4. Güler, Ö.; Bağcı, N. A short review on mechanical properties of graphene reinforced metal matrix composites. *J. Mater. Res. Technol.* **2020**, *9*, 6808–6833. [CrossRef]
5. Kumar, R.; Singh, D.P.; Muñoz, R.; Amami, M.; Singh, R.K.; Singh, S.; Kumar, V. Graphene-based materials for biotechnological and biomedical applications: Drug delivery, bioimaging and biosensing. *Mater. Today Chem.* **2023**, *33*, 101750. [CrossRef]
6. Islam, M.A.; Hossain, A.; Hossain, N.; Ahmed, M.M.S.; Islam, S.; Henaish, A.M.A.; Soldatov, A.V.; Chowdhury, M.A. Recent achievement of graphene in biomedicine: Advancements by integrated microfluidics system and conventional techniques. *Sens. Int.* **2024**, *5*, 100293. [CrossRef]
7. Malisz, K.; Świeczko-Żurek, B. Graphene Production and Biomedical Applications: A Review. *Crystals* **2023**, *13*, 1413. [CrossRef]
8. Devi, N.; Kumar, R.; Singh, S.; Singh, R.K. Recent development of graphene-based composite for multifunctional applications: Energy, environmental and biomedical sciences. *Crit. Rev. Solid State Mater. Sci.* **2024**, *49*, 72–140. [CrossRef]
9. Farjadian, F.; Abbaspour, S.; Sadatlu, M.A.A.; Mirkiani, S.; Ghasemi, A.; Hoseini-Ghahfarokhi, M.; Mozaffari, N.; Karimi, M.; Hamblin, M.R. Recent Developments in Graphene and Graphene Oxide: Properties, Synthesis, and Modifications: A Review. *ChemistrySelect* **2020**, *5*, 10200–10219. [CrossRef]

10. Borane, N.; Boddula, R.; Odedara, N.; Singh, J.; Andhe, M.; Patel, R. Comprehensive review on synthetic methods and functionalization of graphene oxide: Emerging Applications. *Nano-Struct. Nano-Objects* **2024**, *39*, 101282. [CrossRef]
11. Razaq, A.; Bibi, F.; Zheng, X.; Papadakis, R.; Jafri, S.H.M.; Li, H. Review on Graphene-, Graphene Oxide-, Reduced Graphene Oxide-Based Flexible Composites: From Fabrication to Applications. *Materials* **2022**, *15*, 1012. [CrossRef]
12. Daniyal, M.; Liu, B.; Wang, W. Comprehensive Review on Graphene Oxide for Use in Drug Delivery System. *Curr. Med. Chem.* **2020**, *27*, 3665–3685. [CrossRef] [PubMed]
13. Saharan, R.; Paliwal, S.K.; Tiwari, A.; Tiwari, V.; Singh, R.; Beniwal, S.K.; Dahiya, P.; Sagadevan, S. Exploring graphene and its potential in delivery of drugs and biomolecules. *J. Drug Deliv. Sci. Technol.* **2023**, *84*, 104446. [CrossRef]
14. Lee, S.Y.; Kwon, M.; Raja, I.S.; Molkenova, A.; Han, D.-W.; Kim, K.S. Graphene-Based Nanomaterials for Biomedical Imaging. *Adv. Exp. Med. Biol.* **2022**, *1315*, 125–148. [CrossRef]
15. Shankar, K.; Agarwal, S.; Mishra, S.; Bhatnagar, P.; Siddiqui, S.; Abrar, I. A review on antimicrobial mechanism and applications of graphene-based materials. *Biomater. Adv.* **2023**, *150*, 213440. [CrossRef] [PubMed]
16. Echeverri, D.; Calucho, E.; Marrugo-Ramírez, J.; Álvarez-Diduk, R.; Orozco, J.; Merkoçi, A. Capacitive immunosensing at gold nanoparticle-decorated reduced graphene oxide electrodes fabricated by one-step laser nanostructuration. *Biosens. Bioelectron.* **2024**, *252*, 116142. [CrossRef]
17. Zielińska-Górska, M.; Sosnowska-Ławnicka, M.; Jaworski, S.; Lange, A.; Daniluk, K.; Nasiłowska, B.; Bartosewicz, B.; Chwalibog, A.; Sawosz, E. Silver Nanoparticles and Graphene Oxide Complex as an Anti-Inflammatory Biocompatible Liquid Nano-Dressing for Skin Infected with *Staphylococcus aureus*. *J. Inflamm. Res.* **2023**, *16*, 5477–5493. [CrossRef]
18. Prasad, K.; Lekshmi, G.S.; Ostrikov, K.; Lussini, V.; Blinco, J.; Mohandas, M.; Vasilev, K.; Bottle, S.; Bazaka, K. Synergic bactericidal effects of reduced graphene oxide and silver nanoparticles against Gram-positive and Gram-negative bacteria. *Sci. Rep.* **2017**, *7*, 1591. [CrossRef]
19. Oktay, B. Graphene-based materials for bone tissue engineering. *Sigma J. Eng. Nat. Sci.–Sigma Mühendislik Ve Fen Bilim. Derg.* **2024**, *42*, 289–305. [CrossRef]
20. Vasilopoulos, V.; Pitou, M.; Fekas, I.; Papi, R.; Ouranidis, A.; Pavlidou, E.; Patsalas, P. Graphene-Wrapped Copper Nanoparticles: An Antimicrobial and Biocompatible Nanomaterial with Valuable Properties for Medical Uses. *ACS Omega* **2020**, *5*, 26329–26334. [CrossRef]
21. Ismail, A.; Shameli, K.; Ali, R.R.; Sukri, S.N.A.M.; Isa, E.D.M. Copper/Graphene Based Materials Nanocomposites and Their Antibacterial Study: A Mini Review. *J. Res. Nanosci. Nanotechnol.* **2021**, *1*, 44–52. [CrossRef]
22. Lage, T.; Rodrigues, R.O.; Catarino, S.; Gallo, J.; Bañobre-López, M.; Minas, G. Graphene-Based Magnetic Nanoparticles for Theranostics: An Overview for Their Potential in Clinical Application. *Nanomaterials* **2021**, *11*, 1073. [CrossRef] [PubMed]
23. Demirel, E.; Karaca, E.; Durmaz, Y.Y. Effective PEGylation method to improve biocompatibility of graphene derivatives. *Eur. Polym. J.* **2020**, *124*, 109504. [CrossRef]
24. Chen, J.; Liu, H.; Zhao, C.; Qin, G.; Xi, G.; Li, T.; Wang, X.; Chen, T. One-step reduction and PEGylation of graphene oxide for photothermally controlled drug delivery. *Biomaterials* **2014**, *35*, 4986–4995. [CrossRef]
25. Samadian, H.; Mohammad-Rezaei, R.; Jahanban-Esfahlan, R.; Massoumi, B.; Abbasian, M.; Jafarizad, A.; Jaymand, M. A de novo theranostic nanomedicine composed of PEGylated graphene oxide and gold nanoparticles for cancer therapy. *J. Mater. Res.* **2020**, *35*, 430–441. [CrossRef]
26. Bao, Y.; Li, H.; He, J.; Song, K.; Yu, H.; Tian, C.; Guo, J.; Zhou, X.; Liu, S. Polyethylene glycol modified graphene oxide-silver nanoparticles nanocomposite as a novel antibacterial material with high stability and activity. *Colloids Surf. B Biointerfaces* **2023**, *229*, 113435. [CrossRef]
27. Qi, Z.; Shi, J.; Zhang, Z.; Cao, Y.; Li, J.; Cao, S. PEGylated graphene oxide-capped gold nanorods/silica nanoparticles as multifunctional drug delivery platform with enhanced near-infrared responsiveness. *Mater. Sci. Eng. C* **2019**, *104*, 109889. [CrossRef]
28. Cheong, Y.-K.; Arce, M.P.; Benito, A.; Chen, D.; Crisóstomo, N.L.; Kerai, L.V.; Rodríguez, G.; Valverde, J.L.; Vadalia, M.; Cerpa-Naranjo, A.; et al. Synergistic Antifungal Study of PEGylated Graphene Oxides and Copper Nanoparticles against Candida albicans. *Nanomaterials* **2020**, *10*, 819. [CrossRef]
29. Ismail, M.W.; Danial, W.H.; Isa, A.F. Novel approach in synthesizing graphene oxide grafted polyethylene glycol via Steglich Esterification. *Polym. Bull.* **2023**, *80*, 4139–4152. [CrossRef]
30. Karki, N.; Tiwari, H.; Tewari, C.; Rana, A.; Pandey, N.; Basak, S.; Sahoo, N.G. Functionalized graphene oxide as a vehicle for targeted drug delivery and bioimaging applications. *J. Mater. Chem. B* **2020**, *8*, 8116–8148. [CrossRef]
31. Sharma, H.; Mondal, S. Functionalized Graphene Oxide for Chemotherapeutic Drug Delivery and Cancer Treatment: A Promising Material in Nanomedicine. *Int. J. Mol. Sci.* **2020**, *21*, 6280. [CrossRef] [PubMed]
32. Farani, M.R.; Khadiv-Parsi, P.; Riazi, G.H.; Ardestani, M.S.; Rad, H.S. PEGylation of graphene/iron oxide nanocomposite: Assessment of release of doxorubicin, magnetically targeted drug delivery and photothermal therapy. *Appl. Nanosci.* **2020**, *10*, 1205–1217. [CrossRef]
33. Asim, N.; Su'ait, M.S.; Badiei, M.; Mohammad, M.; Akhtaruzzaman, M.; Rajabi, A.; Amin, N.; Ghazali, M.J. Perspectives in biopolymer/graphene-based composite application: Advances, challenges, and recommendations. *Nanotechnol. Rev.* **2022**, *11*, 1525–1554. [CrossRef]

34. Roldán-Matilla, M.; Irigo, P.; Rojas, M.L.; Arce. M., P.; Pérez, J.; Gilsanz-Muñoz, M.F.; Lado-Touriño, I.; Cerpa-Naranjo, A.; Ren, G. Structural Characterisation and Dynamic Modelling of Pegylated Graphene Oxide with Ag and Cu Cluster. *Appl. Surf. Sci.* 2024. *under review*. Available online: https://papers.ssrn.com/sol3/papers.cfm?abstract_id=4979268 (accessed on 17 December 2024).
35. Kalyva, K.; Michalarou, K.; Al Maruf, M.I.H.; Georgakilas, V.I. Graphene Xerogel for Drug Release. *C* **2024**, *10*, 99. [CrossRef]
36. Lima-Sousa, R.; de Melo-Diogo, D.; Alves, C.G.; Costa, E.C.; Ferreira, P.; Louro, R.O.; Correia, I.J. Hyaluronic acid functionalized green reduced graphene oxide for targeted cancer photothermal therapy. *Carbohydr. Polym.* **2018**, *200*, 93–99. [CrossRef]
37. Chen, B.; Liu, M.; Zhang, L.; Huang, J.; Yao, J.; Zhang, Z. Polyethylenimine-functionalized graphene oxide as an efficient gene delivery vector. *J. Mater. Chem.* **2011**, *21*, 7736. [CrossRef]
38. Bao, S.; Yang, W.; Wang, Y.; Yu, Y.; Sun, Y.; Li, K. PEI grafted amino-functionalized graphene oxide nanosheets for ultrafast and high selectivity removal of Cr(VI) from aqueous solutions by adsorption combined with reduction: Behaviors and mechanisms. *Chem. Eng. J.* **2020**, *399*, 125762. [CrossRef]
39. Su, Q.-W.; Lu, H.; Zhang, J.-Y.; Zhang, L.-Z. Fabrication and analysis of a highly hydrophobic and permeable block GO-PVP/PVDF membrane for membrane humidification-dehumidification desalination. *J. Memb. Sci.* **2019**, *582*, 367–380. [CrossRef]
40. Masoumparast, M.; Mokhtary, M.; Kefayati, H. Preparation and characterization of polyvinylpyrrolidone/cobalt ferrite functionalized chitosan graphene oxide ($CoFe_2O_4$ @CS@GO-PVP) nanocomposite. *J. Polym. Eng.* **2020**, *40*, 342–349. [CrossRef]
41. Makharza, S.; Cirillo, G.; Bachmatiuk, A.; Ibrahim, I.; Ioannides, N.; Trzebicka, B.; Hampel, S. Graphene oxide-based drug delivery vehicles: Functionalization, characterization, and cytotoxicity evaluation. *J. Nanopart. Res.* **2013**, *15*, 2099. [CrossRef]
42. Claudio-Rizo, J.A.; Salazar, L.F.C.; Flores-Guia, T.E.; Cabrera-Munguia, D.A. Estructuras metal-orgánicas (MOFs) nanoestructuradas para la liberación controlada de fármacos. *Mundo Nano Rev. Interdiscip. Nanociencias Nanotecnología* **2020**, *14*, 1e–29e. [CrossRef]
43. García-Rodríguez, D.E.; Mendoza-Huizar, L.H.; Díaz, C. A DFT study of Cu nanoparticles adsorbed on defective graphene. *Appl. Surf. Sci.* **2017**, *412*, 146–151. [CrossRef]
44. Fatima, K.; Pandith, A.H.; Manzoor, T.; Qureashi, A. DFT Studies on a Metal Oxide@Graphene-Decorated D$-\pi_1-\pi_2-$A Novel Multi-Junction Light-Harvesting System for Efficient Dye-Sensitized Solar Cell Applications. *ACS Omega* **2023**, *8*, 8865–8875. [CrossRef] [PubMed]
45. Jadoon, T.; Mahmood, T.; Ayub, K. DFT study on the sensitivity of silver-graphene quantum dots for vital and harmful analytes. *J. Phys. Chem. Solids* **2021**, *153*, 110028. [CrossRef]
46. Saravanan, M.; Kandasamy, M.; Suresh, K.; Chakraborty, B.; George, S.D.; Girisun, T.C.S.; Potheher, I.V. Noble metals functionalized reduced graphene oxide as an efficient optical limiter: A combined experimental and theoretical investigation. *Carbon Lett.* **2024**, *34*, 1817–1831. [CrossRef]
47. Shariatinia, Z.; Mazloom-Jalali, A. Molecular dynamics simulations on chitosan/graphene nanocomposites as anticancer drug delivery using systems. *Chin. J. Phys.* **2020**, *66*, 362–382. [CrossRef]
48. Fatema, K.N.; Sagadevan, S.; Cho, J.Y.; Jang, W.K.; Oh, W.-C. Graphene-based nanocomposite using new modeling molecular dynamic simulations for proposed neutralizing mechanism and real-time sensing of COVID-19. *Nanotechnol. Rev.* **2022**, *11*, 1555–1569. [CrossRef]
49. Böyükata, M.; Belchior, J.C. Structural and energetic analysis of copper clusters: MD study of Cu n (n = 2–45). *J. Braz. Chem. Soc.* **2008**, *19*, 884–893. [CrossRef]
50. Rao, Y.; Lei, Y.; Cui, X.; Liu, Z.; Chen, F. Optical and magnetic properties of Cu-doped 13-atom Ag clusters. *J. Alloys Compd.* **2013**, *565*, 50–55. [CrossRef]
51. Biovia Materials Studio, an Integrated, Multi-Scale Modelling Environment. Available online: https://www.3ds.com/products-services/biovia/products/molecular-modeling-simulation/biovia-materials-studio (accessed on 17 December 2024).
52. Hoover, W.G. Canonical dynamics: Equilibrium phase-space distributions. *Phys. Rev. A* **1985**, *31*, 1695–1697. [CrossRef]
53. Nosé, S. A molecular dynamics method for simulations in the canonical ensemble. *Mol. Phys.* **1984**, *52*, 255–268. [CrossRef]
54. Sun, H.; Ren, P.; Fried, J.R. The COMPASS force field: Parameterization and validation for phosphazenes. *Comput. Theor. Polym. Sci.* **1998**, *8*, 229–246. [CrossRef]
55. Mirhosseini, M.M.; Rahmati, M.; Zargarian, S.S.; Khordad, R. Molecular dynamics simulation of functionalized graphene surface for high efficient loading of doxorubicin. *J. Mol. Struct.* **2017**, *1141*, 441–450. [CrossRef]
56. Cha, J.; Kyoung, W.; Song, K.; Park, S.; Lim, T.; Lee, J.; Kang, H. Quantitative Evaluation of the Dispersion of Graphene Sheets with and Without Functional Groups Using Molecular Dynamics Simulations. *Nanoscale Res. Lett.* **2016**, *11*, 136. [CrossRef] [PubMed]
57. Metzler, R.; Jeon, J.-H.; Cherstvy, A.G.; Barkai, E. Anomalous diffusion models and their properties: Non-stationarity, non-ergodicity, and ageing at the centenary of single particle tracking. *Phys. Chem. Chem. Phys.* **2014**, *16*, 24128–24164. [CrossRef]
58. Oliveira, F.A.; Ferreira, R.M.S.; Lapas, L.C.; Vainstein, M.H. Anomalous Diffusion: A Basic Mechanism for the Evolution of Inhomogeneous Systems. *Front. Phys.* **2019**, *7*, 18. [CrossRef]
59. Plimpton, S. Fast Parallel Algorithms for Short-Range Molecular Dynamics. *J. Comput. Phys.* **1995**, *117*, 1–19. [CrossRef]
60. Mahdavi, M.; Fattahi, A.; Tajkhorshid, E.; Nouranian, S. Molecular Insights into the Loading and Dynamics of Doxorubicin on PEGylated Graphene Oxide Nanocarriers. *ACS Appl. Bio Mater.* **2020**, *3*, 1354–1363. [CrossRef]
61. Gervilla, V.; Zarshenas, M.; Sangiovanni, D.G.; Sarakinos, K. Anomalous versus Normal Room-Temperature Diffusion of Metal Adatoms on Graphene. *J. Phys. Chem. Lett.* **2020**, *11*, 8930–8936. [CrossRef]

62. Zarshenas, M.; Gervilla, V.; Sangiovanni, D.G.; Sarakinos, K. Room-temperature diffusion of metal clusters on graphene. *Phys. Chem. Chem. Phys.* **2021**, *23*, 13087–13094. [CrossRef]
63. Manadé, M.; Viñes, F.; Illas, F. Transition metal adatoms on graphene: A systematic density functional study. *Carbon* **2015**, *95*, 525–534. [CrossRef]
64. Chen, Y.-J.; Lee, Y.-T.; Yeh, P.-L.; Wang, B.-C. Optimized geometry, electronic structure and Ag adsorption property of nanosheet graphene with different symmetry shapes: A theoretical investigation. *Res. Chem. Intermed.* **2017**, *43*, 3613–3620. [CrossRef]
65. Mashhadzadeh, A.H.; Vahedi, A.M.; Ardjmand, M.; Ahangari, M.G. Investigation of heavy metal atoms adsorption onto graphene and graphdiyne surface: A density functional theory study. *Superlattices Microstruct.* **2016**, *100*, 1094–1102. [CrossRef]

Disclaimer/Publisher's Note: The statements, opinions and data contained in all publications are solely those of the individual author(s) and contributor(s) and not of MDPI and/or the editor(s). MDPI and/or the editor(s) disclaim responsibility for any injury to people or property resulting from any ideas, methods, instructions or products referred to in the content.